

https://doi.org/10.1070/QEL16504

Broadening and shift of emission lines in a plasma of filaments generated by a tightly focused femtosecond laser pulse in air

A.A. Ilyin, S.S. Golik, K.A. Shmirko, A.Yu. Mayor, D.Yu. Proschenko, Yu.N. Kulchin

Abstract. **We study the broadening and shift of N I (λ = 746.8 nm) and O I (λ =777.4 nm) lines in a plasma of filaments generated by a tightly focused femtosecond laser pulse (0.9 mJ, 48 fs). It is shown that the dynamic Stark effect makes a major contribution to the broadening and shift of the N I line (λ =746.8 nm). It is found that amplified spontaneous emission of a regenerative amplifier and post-pulses break the LS coupling for the O I $3p^5P$ energy level, lead to the generation of side bands related to the Rabi splitting of levels and result in pulsed emission of the first positive system of N_2.**

Keywords: *filament, dynamic Stark effect, Rabi splitting, line broadening and shift.*

1. Introduction

In recent years the study of filamentation processes of femtosecond laser radiation in the atmosphere attracts significant interest [1–4]. In the case of weak focusing or free propagation of a laser beam, the dynamic balance between the processes of plasma defocusing and Kerr self-focusing leads to the formation of a long plasma channel, or a so-called filament with a peak intensity of $\sim 5 \times 10^{13}$ W cm^{-2}. In the case of tight focusing of a laser beam, a major role in the filament formation is played by the geometric focusing, the intensity of the laser radiation in the focal point exceeding 5×10^{13} W cm^{-2} [5]. Moreover, in the case of tight focusing of laser pulses due to lens aberrations, a complex pattern of the radiation intensity distribution having a form of a glowing cone-shaped structure is observed [6].

The plasma of filaments generated by femtosecond pulses is characterised by low temperatures and electron concentrations [7, 8]. These features cause a low emission intensity of the continuous spectrum, intense molecular emission and short lifetime of emission lines. The temporal characteristics of the filament radiation in air depend on the duration τ of the initial ultrashort pulse. For example, for τ = 500 fs at the initial stage the molecular components dominate in the emission of the filament plasma, followed by the continuum emission, then a few nanoseconds later the continuous spectrum is replaced with atomic lines [9]. At τ = 48 fs the continuous spectrum has a very low intensity, the molecular lines are observed immediately after the action of laser radiation, while the atomic lines appear with a delay of 50–80 ps [6]. As shown in Refs [6, 9], in the emission spectrum of filaments one can observe unresolved and abnormally broadened triplets N I ($3p\,^4S-3s\,^4P$) and O I ($3p\,^5P-3s\,^5S$). Earlier Martin et al. [9] with the data of Ref. [10] taken into account supposed that the observed broadening of lines is due to the saturation effect. It is also worth noting that the extremely high value of the parameter of Stark broadening by an electron impact for the O I line (777.4 nm) in the plasma of filaments was experimentally determined in Ref. [11]. The authors give the following explanation to this fact: "the unknown mechanism of broadening of the oxygen atom line can be related to its high chemical activity". At the same time, in the scientific literature there are no papers considering anomalously broadened lines at the initial stages of the filament plasma development, except for papers [6, 9, 11]. Thus, the aim of the present paper is to study the dynamics of broadening and shift of the triplet N I ($3p\,^4S-3s\,^4P$) and O I ($3p\,^5P-3s\,^5S$) lines and to determine the mechanism responsible for the large broadenings and shifts.

2. Experimental setup

Figure 1 presents a schematic of the experimental setup for studying the spectral and temporal characteristics of the plasma emission and the laser pulse passed through the filament. The laser radiation was generated by a Tsunami + Spifire Pro 40F-1W Ti:sapphire laser system (*1*) (the centre wavelength λ = 800 nm, the spectral FWHM 35 nm); the output beam diameter amounted to 7 mm. The filament (*4*) was formed in air, where the lens (*3*) (f = 5 cm) focused the femtosecond pulses (*2*) (the pulse duration 48 fs, the energy 0.9 mJ, the peak power 18 GW, the repetition rate 1 kHz). The spectrum of the laser pulse was approximated by a Gaussian function. The plasma radiation was projected on the input slit of a Spectra Pro 2500i spectrograph (*7*) (Princeton Instruments) by a silica lens (*5*). To suppress the spectral lines in the second order of the diffraction grating, a KS15 filter (*6*) was installed in front of the spectrograph slit. The instrument function width of the spectrograph amounted to 0.34 nm. The filament plasma radiation was recorded at the angle 90° to the direction of the laser beam propagation.

A.A. Ilyin, S.S. Golik, K.A. Shmirko, A.Yu. Mayor, Yu.N. Kulchin Institute of Automation and Control Processes, Far Eastern Branch, Russian Academy of Sciences, ul. Radio 5, 690041 Vladivostok, Russia; Far Eastern Federal University, ul. Sukhanova 8, 690091 Vladivostok, Russia; e-mail: triplecks@mail.ru, golik_s@mail.ru, kshmirko@dvo.ru;
D.Yu. Proschenko Institute of Automation and Control Processes, Far Eastern Branch, Russian Academy of Sciences, ul. Radio 5, 690041 Vladivostok, Russia; Far Eastern Federal University, ul. Sukhanova 8, 690091 Vladivostok, Russia; G.I. Nevelskoi Maritime State University, ul. Verkhneportovaya 50a, 690059 Vladivostok, Russia; e-mail: dima.prsk@mail.ru

Received 29 August 2017; revision received 12 October 2017
Kvantovaya Elektronika **48** (2) 149–156 (2018)
Translated by V.L. Derbov

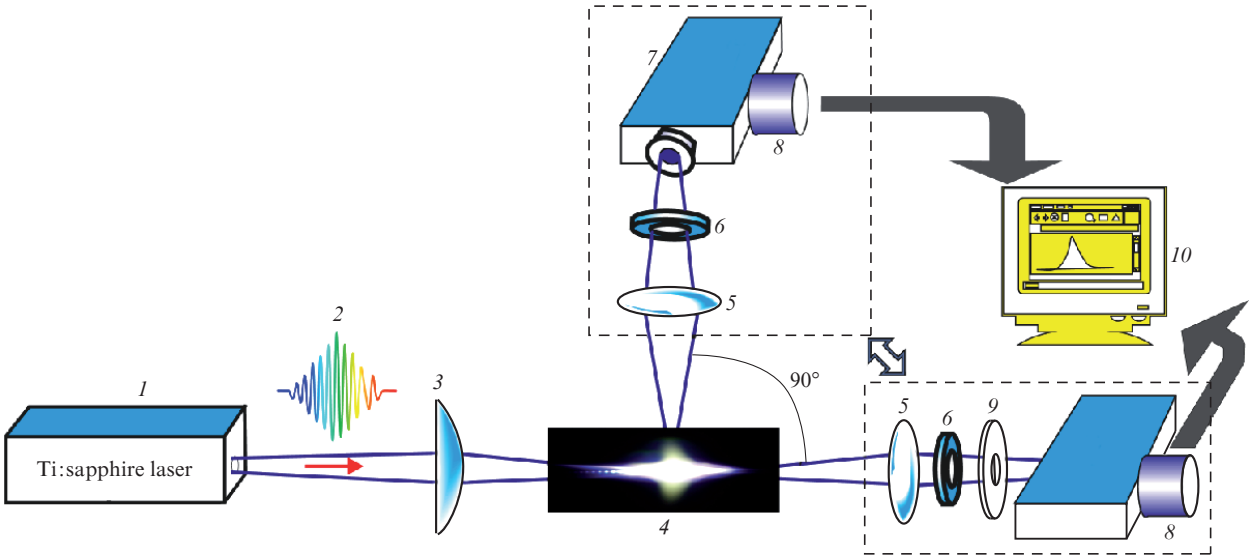

Figure 1. Schematic of the experimental setup.

A PicoStar HR gated ICCD camera (*8*) (12 bit, La Vision) served as a radiation detector. In the registration of the triplets N I ($3p^4S-3s^4P$) and O I ($3p^5P-3s^5S$) we used an exposure of 0.2 ns with a delay step of 1 ns. The characteristics of the emission lines are presented in Table 1. The dynamics of intense pulsed emission of the first positive system of nitrogen $B^3\Pi_g-A^3\Sigma_u^+$ was studied with an exposure delay step of 0.1 ns. The diameter d_{pl} of the plasma channel was estimated from Fig. 3a of Ref. [6] and amounted to ~60 μm. According to Ref. [9], the diameter of the laser beam in the focal point of the lens is $d_{las} = \sqrt{k}\, d_{pl}$. The number of photons k necessary for the ionisation of oxygen and nitrogen molecules was determined from the dependence of the ionisation rate on the intensity of laser radiation (see Ref. [12]). In the range of intensities $5\times10^{13}-2\times10^{14}$ W cm^{-2} we obtained $k(N_2) \approx 5.97$ and $k(O_2) \approx 4.77$. The mean number of photons necessary to ionise an air molecule was determined using the formula $k = k(N_2)h(N_2) + k(O_2)h(O_2)$, where h is the relative contribution to the air ionisation adopted from Ref. [12]. As a result, for the laser pulse energy $E = 0.9$ mJ and duration $\tau = 48$ fs the peak intensity is found to be equal to $I = 4\ln 2E/(\tau\pi d_{las}^2) \approx 9\times10^{13}$ W cm^{-2}.

In the study of the emission dynamics of atomic lines, we found strong pulsed emission of the first positive system of nitrogen, caused by the Rabi splitting of the oxygen atom energy levels in a strong laser field. We recorded for the first time this behaviour of the molecular nitrogen emission in the process of filamentation in air. To check that the radiation is not an artefact, the experimental setup was modified. The system (*1*) was replaced with a Tsunami + Spifire Pro 40F-5W system with an additional double-pass amplifier (800 nm, 65 fs, 1.7 mJ), and the spectrograph (*7*) and the ICCD camera (*8*) were replaced with a Spectra Pro 2300i spectrograph and a PiMax3 camera (16 bit). The laser radiation was focused using the same lens (*5*). The new geometry of the experiment allowed one to record the spectrum of laser pulses passed through the filament and the side satellite related to the Rabi splitting of the O I levels. To avoid the saturation and blooming of the ICCD camera by the laser radiation, we used a CC1 filter (*9*) with an attenuation coefficient nearly constant in the range from 700 to 850 nm. The Pi-Max3 ICCD camera has a wide dynamic range, which allowed the recording of spectral lines weak as compared to the intense line of laser radiation. The radiation passed through the filament was recorded with an exposure of 3 ns.

Table 1. Characteristics of emission lines.

Atom	λ/nm	Energy of the term/eV	Transition	Line strength (a.u.)
N I	742.4	12–10.73	$3p^4S_{3/2}-3s^4P_{1/2,3/2,5/2}$	4.56
	744.3			9.73
	746.8			16.13
O I	777.19	10.73–9.14	$3p^5P_{3,2,1}-3s^5S_2$	59.9
	777.42			42.8
	777.54			25.7

3. Results and discussion

3.1. Broadening and shift of lines

As mentioned above, Ilyin et al. [6] observed an anomalously broadened line, the characteristics of which are presented in Table 1. Figure 2 shows the dynamics of the line shift and broadening, recorded in Ref. [6]. For oxygen atoms the broadening and shift correspond to the unresolved triplet O I (777.4 nm), for nitrogen – to the most intense line N I (746.8 nm). The line shift was calculated as follows: at $t >$ 110 ns the mean value of the line centre was determined, which then was subtracted from the value of the line centre at $0 < t < 150$ ns. At $t > 110$ ns the lines were considered unshifted for the following reasons. First, the numerical modelling shows that for $I = 8\times10^{13}$ W cm^{-2} and $\tau = 100$ fs the concentration of electrons decreases by three orders of magnitude during 100 ns, while the temperature of air molecules remains virtually unchanged [13]. Second, the line width for N I (746.8 nm) is equal to the instrumental width at $t > 100$ ns (Fig. 2b). Therefore, the Stark and Van der Waals mechanisms cannot essentially affect the line shift at $t > 110$ ns.

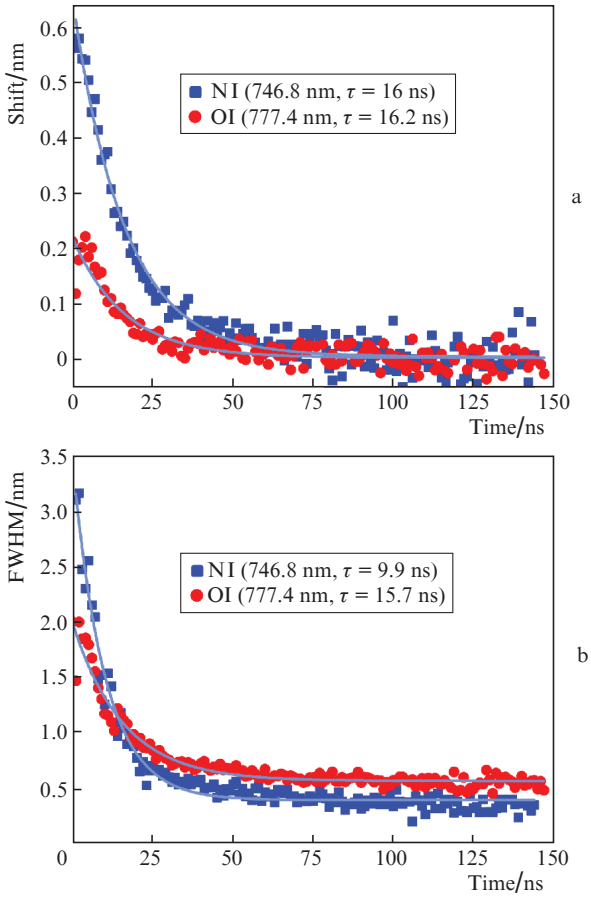

Figure 2. Time dependences of the line shift and broadening. Solid lines are the approximations by exponential functions with the decay time τ.

The O I and N I lines exhibit a red shift and, as was already mentioned above, an extremely large width. The initial shift of the nitrogen line is three times greater than that of the oxygen line, the N I line (746.8 nm) being broader than the O I triplet at $t < 15$ ns. In Ref. [6], it is shown that the filament plasma consists of electrons, molecules, molecular ions and atoms. To determine the effect of different mechanisms on the shift and broadening of lines, it is necessary to estimate the concentrations of the above plasma particles. The concentration of electrons n_e can be estimated in the following way:

$$n_e \approx (R_{O_2}(I)0.21 + R_{N_2}(I)0.79)\tau N,$$

where $R(I)$ is the ionisation rate from Ref. [12] and $N = 2.5 \times 10^{19}$ cm^{-3}. For $I = 9 \times 10^{13}$ W cm^{-2} and $\tau = 48$ fs we obtain $n_e \approx 8 \times 10^{17}$ cm^{-3}. Allowing for a fast decrease in the electron concentration, we assume in further estimates that during the first nanoseconds the mean concentration of electrons is $n_e = 5 \times 10^{17}$ cm^{-3}. These times correspond to large values of the width and shift (Fig. 2). The model of plasma dynamics for filamentation in air presented in Ref. [14] yields the following concentration of particles at $I = 4 \times 10^{13}$ W cm^{-2} and $t \approx 1$ ns: $n_O \sim 5 \times 10^{16}$ cm^{-3} and $n_N \sim 5 \times 10^{14}$ cm^{-3}. According to this model, it is possible to take into account that $n(O_2^+) \approx n_e \gg n(N_2^+)$. Thus, we obtain $n(O_2) \approx 5 \times 10^{18}$ cm^{-3} and $n(N_2) \approx 2 \times 10^{19}$ cm^{-3}. The initial temperature of the electrons should be taken equal to $T_e = 10^4$ K, which is close to the temperature of electrons, obtained in Refs [13, 14]. According to Ref. [14], the temperature of heavy particles is $T = 320$ K.

For the filament plasma, the line shift d is caused by the Stark and Van der Waals effects, while the line width w is determined by the instrumental, Doppler, resonance, Van der Waals and Stark broadenings. The widths and shifts of the emission lines, calculated using the formulae from Refs [15, 16] and the above values of temperature and concentration, are presented in Table 2. The polarisabilities of atoms and molecules, necessary for calculating the Van der Waals broadening, were borrowed from Refs [17, 18]. According to the presented data, the major contribution to the line shift is introduced by the Stark effect, while the broadening is determined by the instrumental and Stark mechanisms, which agrees with the results of Refs [9, 11]. However, the data of Table 2 do not explain the maximal values of the line width and shift in Fig. 2.

Martin et al. [9] made a suggestion that the saturation broadening is a cause of the large line widths. According to Siegman [10], the saturated line half-width is expressed as $\Delta\nu_b = \Delta\nu_a \times \sqrt{1 + I/I_{sat}}$, where $\Delta\nu_a$ is the line half-width in the absence of saturation (in our case caused by the electron impact broadening); I is the line radiation intensity; and $I_{sat} = h\nu/(\sigma\tau_{eff})$ is the saturation intensity. Martin et al. [9] state that for the filament plasma $I \gg I_{sat}$, which leads to the line broadening. The cross section of induced emission is given by the relation $\sigma = \gamma_r\lambda^2/(2\pi)^2\Delta\nu_a$, where γ_r is the probability of a spontaneous transition [6]. The time of recovery of the level populations is $\tau_{eff} = (\gamma_1 + \gamma_{20})/(\gamma_1\gamma_2)$, where γ_1 and $\gamma_2 = \gamma_{21} + \gamma_{20}$ are the rates of transition of the particles from the lower laser level 1 ($3s\,^5S$) and the upper laser level 2 ($3p\,^5P$) to all lower levels [10]. The energy level diagram of the oxygen atom is presented in Fig. 3. The rate γ_{21} corresponds to the transition $3p\,^5P - 3s\,^5S$, the rate γ_{20} to the transition $3p\,^5P - 2p^4\,^3P$, and the rate γ_1 to the transition $3p\,^5S - 2p^4\,^3P$. The radiative transitions to the ground state are forbidden by the selection rules. The transitions from the 'laser' levels to the levels $2p^4\,^1D$ and $2p^4\,^1S$ have zero cross sections [19]. The rate of the particle departure is expressed as follows:

$$\gamma_{ji} = k_{ij}\frac{g_i}{g_j}\exp\left(\frac{E_j - E_i}{T_e}\right)n_e,$$

where k_{ij} are the excitation rate constants from Ref. [19] and E is the energy of the level.

The calculations show that $\gamma_1 \approx \gamma_{20}, \gamma_{21} \gg \gamma_{20}$, and $\gamma_{21} \gg \gamma_r$. Therefore, $\tau_{eff} \approx 2/\gamma_{21}$, and the saturation intensity is $I_{sat} \approx 1.7 \times 10^6$ W cm^{-2}. The maximal intensity $I_{max} = \Delta N_0 h\nu L/\tau_{eff}$,

Table 2. Widths (w) and shifts (d) jf lines.

Atom	λ/nm	Stark/nm		Van der Waals/nm		Resonance/nm	Doppler/nm	Instrumental/nm
		w_S	d_S	w_V	d_V	w_{res}	w_D	w_{inst}
N I	746.8	0.48	0.25	0.04	0.027	5.9×10^{-6}	2.6×10^{-3}	0.34
O I	777.4	0.32	0.07	0.035	0.023	–	2.5×10^{-3}	

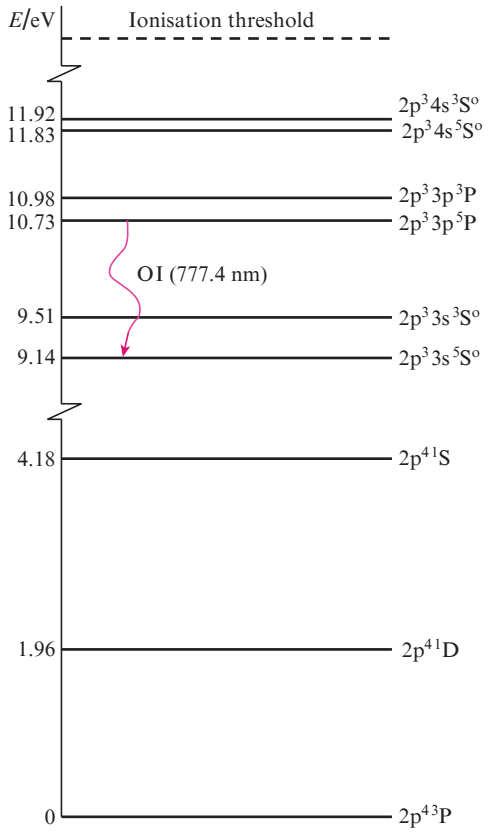

Figure 3. Energy level diagram of O I.

where L is the size of the medium, in which the radiation is generated; and ΔN_0 is the unsaturated population inversion. In Ref. [9] the oxygen line was recorded in the transverse direction; therefore, $L \sim d_{pl}/2 = 0.1$ mm. In the spectra presented in Refs [6, 9], the N II and O II lines are absent, i.e., the recombination pumping of the levels $3p\,^5P$ and $3s\,^5S$ is negligibly small. Thus, the oxygen atoms are initially generated in the ground state via the reaction of dissociative recombination [20], after which the transition to the levels $3p\,^5P$ and $3s\,^5S$ occurs. Assuming that $\Delta N_0 \sim n(3s\,^5S)$ and that the population distribution for the levels $3s\,^5S$ and $2p^4\,^3P$ is a Boltzmann one, we obtain $I_{max} \approx 80$ W cm^{-2}. Thus, the assumption $I \gg I_{sat}$ of Ref. [9] appears to be incorrect, and the large line widths cannot be explained by the saturation effect.

3.2. Side satellite generation

To clarify the mechanism of large emission line widths in the process of filamentation, the step of the exposure delay was reduced to 0.1 ns. In some cases the high-power pulsed emission of the first positive system of $N_2(B\,^3\Pi_g - A\,^3\Sigma_u^+)$ was observed that has not been previously reported. The time-resolved images of the plasma emission spectrum are presented in Fig. 4. The rounded lower corners of the images are due to the partial overlap of the ICCD matrix and the photocathode. At $t = 0.1$ ns one can see a weak O I line (777.4 nm) and a N_2 (3–1) line with the centre wavelength $\lambda = 760.6$ nm (3 and 1 are the vibration quantum numbers of the upper and lower level, respectively), as reported in Ref. [6]. The emission spectrum consists of two spatially separated regions. The most intense region is located closer to the focusing lens. Apparently, the lens aberrations [6] and/or the post-pulses [21] are responsible for the spatial separation of the filament plasma radiation. The strongly broadened triplet N I is formed later (at $t = 0.7$ ns). Then the intensity of the (3–1) line rapidly grows, the line becomes more expressed in comparison with the line O I ($t = 2$ ns), and its intensity reaches a maximal value at $t = 2.5$ ns. At t varying from 2 ns to 3.1 ns in Fig. 2 the following peculiarity is observed: the size of the emission zone of the molecular lines (3–1) and (4–2) rapidly grows and exceeds the initial size of the filament emission zone at $t = 0.1$ ns, while for the atomic lines O I and N I the size of the emission zone remains unchanged. The zone extension is asymmetric, i.e., the emission zone is elongated towards the laser beam. At $t = 2.8$ ns the intensity of the (3–1) line decreases, and the (4–2) line centred at $\lambda = 748.4$ nm becomes more intense. Then the emission of the lines of the first positive system abruptly terminates ($t > 3.1$ ns). The high-power radiation at (3–1) and (4–2) transitions looks as induced radiation with the characteristic time ~1 ns.

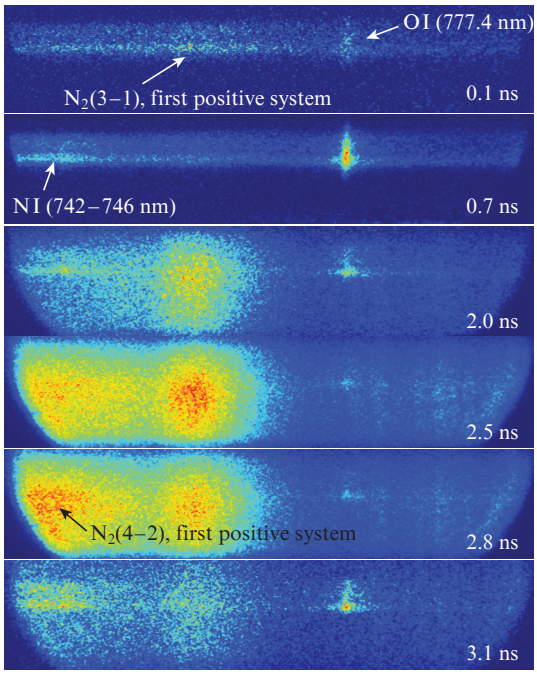

Figure 4. Time-resolved images of the plasma emission spectrum in the range 740–800 nm (3–1 and 4–2 are the vibration quantum numbers). The laser radiation propagates upwards.

The time-resolved spectra of plasma emission corresponding to Fig. 4 are presented in Fig. 5. It is seen that pulsed emission of N_2 molecules is initially accompanied by the broadening of O I lines and by an increase in their intensity. Then the continuum emission, corresponding to the (7–6) transition of the first positive system, 'hides' the oxygen line. Note that the weak pulsed emission of the first positive system was observed in Ref. [6] at $t = 2$ and 3 ns.

This behaviour of the low-intensity first positive system (compared to the second positive and the first negative systems of N_2) is rather strange, since the radiative lifetime of vibration sublevels for the level $B\,^3\Pi_g$ with $v' = 3$ and 4 is equal to 8.3 and 7.5 μs, respectively [22].

The authors of papers [23, 24] observed the broadband satellites, shifted to the blue and to the red with respect to the emission line of the Ti : sapphire laser for the filaments excited

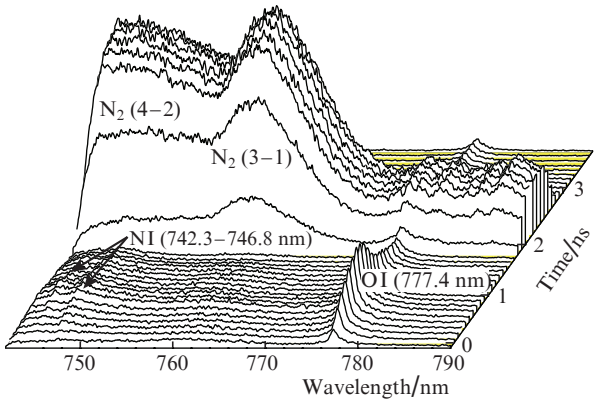

Figure 5. (Colour online) Emission spectrum dynamics of the filament. The background level is shown by the yellow colour.

by a laser pulse in oxygen. The Rabi oscillations were generated at the O I $3p\,^5P-3s\,^5S$ transition by the second laser pulse with $\tau \sim 1$ ps and $I \sim 10^9-10^{10}$ W cm^{-2}. Therefore, in our case the side satellite shifted to the blue and having the intensity by an order of magnitude exceeding the intensity of the red-shifted satellite [23] can give rise to the emission of the (3–1) and (4–2) lines. In our case the second picosecond pulse is absent, but under tight focusing of the radiation the post-pulses and the amplified spontaneous emission in the regenerative amplifier (ASE) [7, 25] possess enough intensity to generate side satellites related to the Rabi splitting of the O I levels. To check the presence of side satellites in the spectrum, the experimental setup was modified as described in Section 2.

The spectrum of the laser radiation passed through the filament is shown in Fig. 6. The time is counted from the maximum of the laser pulse at the wavelength $\lambda = 813$ nm, i.e., the main pulse having the duration 65 fs terminates at $t \approx 1.5$ ns. The spectrum of the main pulse is strongly shifted to the blue and is transformed into three peaks. This behaviour is due to the self-phase modulation in the medium with Kerr and plasma nonlinearities [26]. The intensity of the laser radiation rapidly decreases with time, the time of the side satellite

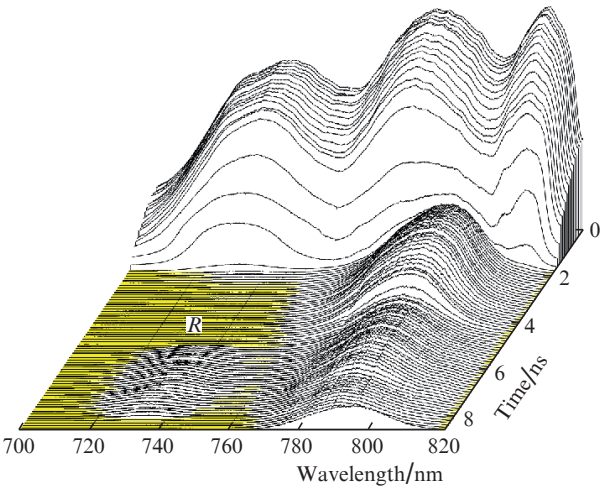

Figure 6. (Colour online) Spectrum of a laser pulse passed through the filament; *R* is the side satellite; the background level is shown by the yellow colour.

appearance being $t = 5.3$ ns, which differs from $t = 1.8$ ns for a smaller energy pulse (see Fig. 4). With allowance for the exposure time equal to 3 ns, one can suppose that the duration of side satellite emission does not exceed 3 ns. In the new geometry of the experiment, the side satellite with the centre at the wavelength $\lambda \approx 735$ nm is shifted with respect to the emission lines of N_2, 760.6 nm (3–1) and 748.4 nm (4–2). At $t > 2$ ns, in Fig 6 one can observe the blue shift of the laser wavelength amounting to 10–15 nm and decreasing with time.

The interaction of high-power laser radiation at the frequency ω with oxygen atoms near the $3p\,^5P-3s\,^5S$ transition leads to the appearance of side satellites at the frequencies $\omega + \Omega'$. The generalised Rabi frequency is expressed as $\Omega' = \sqrt{\Delta^2 + \Omega^2}$, where Δ is the frequency detuning from the centre frequency of the exciting laser pulse, and $\Omega = \mu F/\hbar$ is the Rabi frequency depending on the reduced dipole matrix element μ and the amplitude of the electric field F. The dipole matrix element is $\mu = \sqrt{\mathcal{S}}$, where $\mathcal{S}$ is the line strength from the NIST database [27] (its values are presented in Table 1). Here and below one should distinguish between the line strength $\mathcal{S}$ and the total spin quantum number S. For a laser pulse with a spectrum shifted to the blue by 10 nm the detuning is $\Delta \approx 0.026$ eV. Note that in the example presented in Fig. 6 the side bands corresponding to the $J' = 3 - J = 2$ and $J' = 2 - J = 2$ transitions are absent. For example, for the $J' = 3 - J = 2$ transition and the intensity $I = 2 \times 10^{10}$ W cm^{-2} the peak in the vicinity of 717 nm should be observed, which contradicts the experimental results presented in Fig. 6 and the results of Refs [23, 24]. Apparently, this contradiction may be explained by the breakdown of the LS coupling for the O I $3p\,^5P$ level in the strong laser field [28–30]. If the perturbation caused by the strong laser field considerably exceeds the spin–orbit coupling, then, according to Ref. [28], the atomic states cannot be described in the basis $|n, L, S, J, M_J\rangle$. At $I \sim 10^{10}$ W cm^{-2} the Rabi splitting is $\hbar\Omega' = 0.08$ eV ($J' = 1 - J = 2$), which is by two orders of magnitude higher than the multiplet splitting $\Delta_{LS} = 7 \times 10^{-4}$ eV for the oxygen atom. Under such conditions the electric field couples with the total orbital angular vector L. According to Ref. [31], $\mathcal{S}$ for the $nlSL-n'l'SL'$ transition is determined by the expression

$$\mathcal{S} = |\langle nL\,\|D\|\,n'L'\rangle|^2 = \frac{1}{2S+1}\sum_{JJ'}\mathcal{S}(lSLJ;l'SL'J'). \qquad (1)$$

From Eqn (1) it is easy to obtain $\mathcal{S} = 25.7$ a.u. Therefore, for $\Delta \approx 0.026$ eV the mean intensity of laser radiation is $I = 2.5 \times 10^{10}$ W cm^{-2} at $5 \leqslant t \leqslant 8$ ns (Fig. 6) and $I = 1.2 \times 10^{10}$ W cm^{-2} at $t = 2.5$ ns (see Fig. 5) (side satellite at $\lambda \approx 750$ nm).

Note that the intensity $I \sim 10^{10}$ W cm^{-2} of the nanosecond component of the femtosecond pulse is sufficient to support the absorption wave (laser-supported detonation wave, fast ionisation wave) in the process of the air breakdown by a nanosecond laser pulse (Fig. 6) [32, 33]. However, in the experiment the breakdown was not observed.

The condition for the breakdown initiation is determined by the following criterion [34]: in the focal volume, there must be at least $10^{13}-10^{14}$ electrons. If we assume the focal volume to be a cylinder with a diameter $d_{pl} = 60$ μm and a length 2 mm [6], then for the electron concentration $n_e = 8 \times 10^{17}$ cm^{-3} we obtain 4.5×10^{12} electrons in the focal volume. Because the volume of the plasma channel is much smaller, we can conclude that in our case the breakdown is impossible.

Using the above results, the pulsed emission of the first positive system can be described in the following way. In the experiment, the repetition rate of the laser pulses amounts to 1 kHz. The $A^3\Sigma_u^+$ level is metastable with the radiation lifetime ~2 s; therefore, the filament is surrounded by $N_2(A^3\Sigma_u^+)$ molecules pushed from the filamentation region by the shock waves generated by the preceding femtosecond pulses. The blue shift of the spectrum of the main femtosecond pulse (Fig. 6) pumps the $B^3\Pi_g$ level, and in a few nanoseconds, the laser field (ASE + post-pulses) generates the side satellites. The more intense component causes the induced radiation and the appearance of intense lines of the first positive system (see Figs 4 and 5). The asymmetry of the emission zone in Fig. 4 can be explained by more intense radiation of side satellites in the backward direction, as well as by the lens aberrations [6].

3.3. Shift and broadening of lines in a strong laser field

The dynamic Stark effect in the near-resonance strong laser field described above leads to the generation of side satellites and to the possible LS-coupling breakdown. For the $3p\,^4S_{3/2}-3s\,^4P_{5/2}$ transition of nitrogen, the detuning Δ = 0.11 eV is much greater than the Rabi frequency $\hbar\Omega'$ = 0.04 eV. Thus, nitrogen is characterised by a nonresonance dynamic Stark effect that changes the atomic level energy by [35–37]

$$\Delta E = -\frac{F^2}{4}\left[\alpha^{\mathrm{s}} + \alpha^{\mathrm{t}}\frac{3M^2 - J(J+1)}{J(2J-1)}\right], \qquad (2)$$

where α^{s} and α^{t} are the dynamic scalar and tensor polarisabilities, respectively; and M is the projection of J. The tensor part in Eqn (2) is responsible for the splitting of the energy level and disappears in the process of averaging over M. Therefore, the line shift d_{f} corresponds to the difference of scalar polarisabilities of the upper (u) and the lower (l) level: $d_{\mathrm{f}} = -\lambda^2F^2(-\alpha_{\mathrm{u}}^{\mathrm{s}} + \alpha_{\mathrm{l}}^{\mathrm{s}})/(4hc)$. Taking into account the shift d_{col} related to the collisions with plasma particles and caused mainly by the Stark effect (see Table 2), the line shift can be expressed as $d = d_{\mathrm{col}} + d_{\mathrm{f}}$. In our case, the laser pulse spectral width amounts to ~35 nm; therefore, d_{f} is determined by the relation:

$$d_{\mathrm{f}} = -1.562\times10^{-19}\lambda^2 I_0\frac{\int_0^\infty g(\varepsilon)[-\alpha_{\mathrm{u}}^{\mathrm{s}}(\varepsilon) + \alpha_{\mathrm{l}}^{\mathrm{s}}(\varepsilon)]\,\mathrm{d}\varepsilon}{\int_0^\infty g(\varepsilon)\,\mathrm{d}\varepsilon}, \qquad (3)$$

where λ is expressed in nanometres and ε is the photon energy. The laser pulse spectrum is approximated by the function $I = I_0 g(\varepsilon)$, where I_0 is the intensity in the line centre (W cm^{-2}) and $g(\varepsilon)$ is the normalised laser pulse spectrum described by the Gaussian function.

In contrast to the O I $3p\,^5P$ level, the N I $3s\,^4P$ level has a much stronger spin–orbit coupling and the separation between the energy level is $\Delta_{\mathrm{LS}} = 10^{-2}$ eV so that α^{s} is determined by the formula [35]:

$$\alpha^{\mathrm{s}} = \frac{\alpha_{nJ}^{(0)}}{\sqrt{3(2J+1)}},$$

$$\alpha_{nJ}^{(K)} = (-1)^{K+J+1}\sqrt{2K+1}\sum_{n'J'}(-1)^{J'} \times\begin{Bmatrix}1 & K & 1\\ J & J' & J\end{Bmatrix}\frac{|\langle n'J'\|\,D\,\|nJ\rangle|^2}{\hbar}\times \qquad (4)$$

$$\times\mathrm{Re}\left(\frac{1}{\omega_{n'J'nJ} - \omega - \mathrm{i}w_{n'J'nJ}/2} + \frac{1}{\omega_{n'J'nJ} + \omega + \mathrm{i}w_{n'J'nJ}/2}\right).$$

In Eqn (4), $\{\ldots\}$ is the Wigner 6j symbol; $\omega_{n'J'nJ}$ is the angular frequency of the $n'J'-nJ$ transition; $w_{n'J'nJ}$ is the width of the lines lying within the laser emission spectrum; and K = 0 and 2 for the scalar and tensor polarisabilities, respectively. To calculate $\alpha_{nJ}^{(K)}$ one needs the values of the line strength and the wavelength for the $n'J'-nJ$ transitions presented in the ASD database [27]. However, for highly excited states and the levels lying above the ionisation potential, such information is absent. Nevertheless, the higher the energy of the level, the smaller the line strength. For example, $\mathcal{S}(3p\,^4S_{3/2} - 3s\,^4P_{5/2})$ = 16.13 a.u. and $\mathcal{S}(4p\,^4S_{3/2} - 3s\,^4P_{5/2})$ = 0.14 a.u. We should emphasise that $\alpha_{nJ}^{(K)}$ in Eqn (4) is inversely proportional to the transition frequency. Thus, we can suppose that the contribution of highly excited sates and the states with the energy exceeding the ionisation threshold is negligibly small. The result of our calculations of the difference of polarisabilities $-\alpha(^4S_{3/2}) + \alpha(^4P_{5/2})$ based on Eqn (4) are shown in Fig. 7. It is seen that within the laser pulse spectrum it is mainly negative, i.e., the N I (746.8 nm) line will be shifted to the red in correspondence with Eqns (3) and (4). In our case, the total shift at t = 1–2 ns equals 0.58 nm (see Fig. 2). By subtracting the collision Stark shift 0.25 nm (Table 2) we obtain a shift of 0.33 nm due to the dynamic Stark effect. For $I = 1.2\times10^{10}$ W cm^{-2} this value corresponds to the blue shift of the laser pulse spectrum by 17 nm.

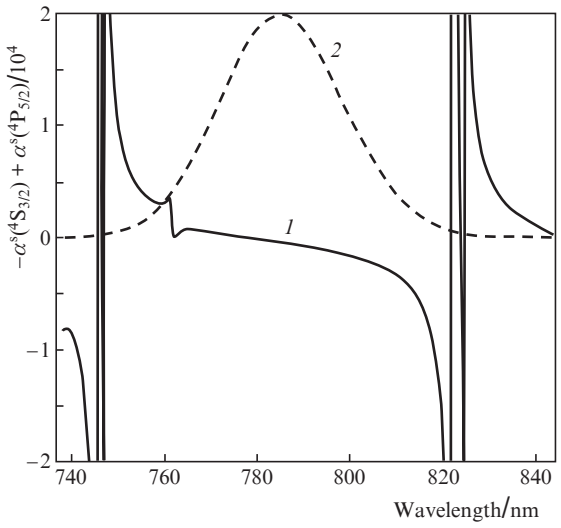

Figure 7. (*1*) Polarisability difference between N I $^4S_{3/2}$ and $^4P_{5/2}$ levels and (*2*) laser pulse spectrum.

Using the results of Ref. [37], the line width in the strong laser field can be estimated as follows:

$$w_{\mathrm{f}} = 3.336\times10^{-18}\lambda^2[w_{\mathrm{f}}(^4S_{3/2}^0) + w_{\mathrm{f}}(^4P_{5/2})],$$

where λ is measured in nanometres and $w_{\mathrm{f}}(^{2S+1}L_J)$ is the level width equal to the separation between the magnetic sublevels of the J level. The level width is determined according to Eqn (3), where $[-\alpha_{\mathrm{u}}^{\mathrm{s}}(\varepsilon) + \alpha_{\mathrm{l}}^{\mathrm{t}}(\varepsilon)]$ is replaced with $3[J(2J-1)]^{-1}\times|\alpha^{\mathrm{t}}(\varepsilon)|(M^2 - M'^2)$, with the difference $M^2 - M'^2$ being maximal. The tensor polarisability is expressed as [35]

$$\alpha^{t} = -\sqrt{\frac{2J(2J-1)}{3(J+1)(2J+1)(2J+3)}}\,\alpha_{nJ}^{(2)}.$$

Thus the line width w_f caused by the splitting of levels in the strong laser field with the intensity $I = 1.2 \times 10^{10}$ W cm^{-2} is equal to 1.98 nm. Assuming the collision Stark broadening to produce a Lorentz line contour, we obtain the final line width $w = 0.534w_L + (0.2169w_L^2 + w_{inst}^2)^{1/2}$ [38], where $w_L = w_{col} + w_f$. Neglecting the Van der Waals broadening, we obtain the total line width $w = 2.51$ nm, which is close to the experimental line width 3.16 nm (see Fig. 2b). This makes it possible to conclude that the level splitting due to the dynamic Stark effect makes the greatest contribution to the line broadening. From the above formula, it is seen that the accuracy of w_f calculation strongly affects the accuracy of the determination of the total line width. The calculations of the line broadening and shift due to the dynamic Stark effect carried out by us are approximate for the following reasons. First, the instantaneous shape of the laser pulse spectrum at the delays 0 – 3 ns is unknown and cannot be approximated by the Gaussian function (Fig. 6). Second, the position of the intensity maximum of the side satellite in Figs 4 and 5 is given approximately, so that the intensity $I = 1.2 \times 10^{10}$ W cm^{-2} is determined approximately too. We should note that at $I = 1.5 \times 10^{10}$ W cm^{-2} the calculated line width is equal to the experimental one (3.16 nm). Thus, the nonresonance dynamic Stark effect and the Stark effect caused by the interaction with charged particles lead to the line broadening and shift in the filament plasma.

For the O I line (777.4 nm) the calculation of broadening and shift as a result of the resonance dynamic Stark effect is a very complicated problem and requires using the density matrix formalism [23], since it is necessary to consider the elastic and inelastic collisions of electrons with atoms depending on the electron temperature and concentration. Nevertheless, some qualitative considerations are possible. The time dependence of the width and shift of lines is well approximated by the function $f(t) = a\exp(-t/\tau) + b$, where τ is the characteristic decay time (see Fig. 3). Except for the width of the N I line (746.8 nm) , the shifts and the width of the O I line (777.4 nm) have nearly similar characteristic times τ = 15.7 – 16.2 ns (Fig. 2). Allowing for the weak temperature dependence of the parameter of the line shift due to the electron impact, we can suppose that the characteristic time of the electron concentration decay amounts to ~16 ns. Therefore, the shift of lines is determined mainly by the electron impact, while the dynamic Stark effect affects the line shift only at the initial moments of filament plasma evolution due to the rapidly decreasing intensity of ASE and post-pulses. The fast decrease in the width of the N I (746.8 nm) line (τ = 10.1 ns, see Fig. 2) is most probably related to the decrease in the laser radiation intensity.

4. Conclusions

We have shown that the broadening and shift of lines emitted under the conditions of filamentation of tightly focused laser pulse in air is caused mainly by the laser field of ASE and post-pulses. This field leads to the breakdown of LS coupling for the O I 3p ^{5}P level, to the generation of side satellites and to the high-power radiation of the first positive system of N_2, not described previously in the scientific literature. The generation of side satellites can become a powerful tool in remote sensing of different media with the radiation of a Ti : sapphire laser, provided that the emission line of the elements comprising the medium is close to the O I line (777.4 nm). One should allow for the fact that the induced radiation of the first positive system can be an obstacle for the detection of the lines of other elements, which was observed in the filaments generated at the water surface [39]. It is also reasonable to detect the lines of elements in femtosecond laser-induced breakdown spectroscopy with a certain delay, at which the laser field of ASE and post-pulses does not affect the contour of the detected lines.

Acknowledgements. The study of the spectral line shifts was carried out in the Far Eastern Federal University under the financial support from the Russian Science Foundation (Project No. 14-50-00034). The analysis of line broadening was supported by the Russian Foundation for Basic Research within Grant No. 17-02-00802A received by S.S. Golik executing the 'Organisation of Scientific Research' programme of the Ministry of Education and Science of the Russian Federation with the help of the unique instrumentation of the 'Laser Methods for Investigating Condensed Media and Biological Objects and Environmental Monitoring' Centre (MAC LAMI) of the Institute of Automation and Control Process, Far Eastern Branch of the Russian Academy of Sciences.

References

1. Chekalin S.V., Kandidov V.P. *Phys. Usp.*, **56** (2), 123 (2013) [*Usp. Fiz. Nauk*, **183**, 133 (2013)].
2. Kandidov V.P., Shlenov S.A., Kosareva O.G. *Quantum Electron.*, **39**, 205 (2009) [*Kvantovaya Elektron.*, **39**, 205 (2009)].
3. Apeksimov D.V., Geints Yu.E., Zemlyanov A.A., Kabanov A.M., Matvienko G.G., Oshlakov V.K. *Quantum Electron.*, **45** (5), 408 (2015) [*Kvantovaya Elektron.*, **45** (5), 408 (2015)].
4. Chin S.L., Wang T.J., Marceau C., Wu J., Liu J.S., Kosareva O., Panov N., Chen Y.P., Daigle J.F., Yuan S., Azarm A., Liu W.W., Seideman T., Zeng H.P., Richardson M., Li R., Xu Z.Z. *Laser Phys.*, **22**, 1 (2012).
5. Lim K., Durand M., Baudelet M., Richardson M. *Sci. Rep.*, **4**, 7217 (2014).
6. Ilyin A.A., Golik S.S., Shmirko K.A. *Spectrochim. Acta B*, **112**, 16 (2015).
7. Labutin T.A., Lednev V.N., Ilyin A.A., Popov A.M. *J. Anal. At. Spectrom.*, **31**, 90 (2016).
8. Musazzi S., Umberto P. (Eds) *Laser-induced Breakdown Spectroscopy: Theory and Applications* (Berlin; Heidelberg: Springer-Verlag, 2014).
9. Martin F., Mawassi R., Vidal F., Gallimberti I., Comtois D., Pépin H., Kieffer J.C., Mercure H.P. *Appl. Spectrosc.*, **56**, 1444 (2002).
10. Siegman A.E. *Lasers* (Mill Valley, California: University Science Books, 1986).
11. Bernhardt J., Liu W., Theberge F., Xu H.L., Daigle J.F., Chateauneuf M., Dubois J., Chin S.L. *Opt. Commun.*, **281**, 1268 (2008).
12. Kasparian J., Sauerbrey R., Chin S.L. *Appl. Phys. B*, **71**, 877 (2000).
13. Henis Z., Milikh G., Papadopoulos K., Zigler A. *J. Appl. Phys.*, **103**, 103111 (2008).
14. Shneider M.N., Zheltikov A.M., Miles R.B. *Phys. Plasmas*, **18**, 063509 (2011).
15. Griem H.R. *Spectral Line Broadening by Plasmas* (New York: Academic, 1974).
16. Konjevic N. *Phys. Rep.*, **316**, 339 (1999).
17. Cox A.N. (Ed.) *Allen's Astrophysical Quantities* (New York: Springer-Verlag, 2002).

18. Olney T.N., Cann N.M., Cooper G., Brion C.E. *Chem. Phys*., **223**, 59 (1997).
19. Barklem P.S. *Astron. Astrophys*., **462**, 781 (2007).
20. Ilyin A.A. *Tech. Phys. Lett*., **42**, 1024 (2016) [*Pis'ma Zh. Tekh. Fiz*., **42**, 1024 (2016)].
21. Nan Z., Wen-Xia B., Jing-Hui Y., Xiao-Nong Z. *Chin. Phys. B*, **22**, 054209 (2013).
22. Chauveau S., Perrin M.-Y., Riviere Ph., Soufiani A. *J. Quant. Spectrosc. Radiat. Transf*., **72**, 503 (2002).
23. Compton R., Filin A., Romanov D.A., Levis R.J. *Phys. Rev. A*, **83**, 053423 (2011).
24. Heck G., Filin A., Romanov D.A., Levis R.J. *Phys. Rev. A*, **87**, 023419 (2013).
25. Keppler S., Savert A., Korner J., Hornung M., Liebetrau H., Hein J., Kaluza M.C. *Laser Photon. Rev*., **10**, 264 (2016).
26. Apeksimov D.V., Bukin O.A., Bykova E.E., Geints Yu.E., Golik S.S., Zemlyanov A.A., Il'in A.A., Kabanov A.M., Matvienko G.G., Oshlakov V.K., Petrov A.V., Sokolova E.B. *Plasma Phys. Rep*., **39**, 1056 (2013).
27. NIST, Atomic Spectra Database, https://www.nist.gov/pml/atomic-spectra-database.
28. Dubreuil B., Chapelle J. *Physica B+ C*, **94**, 233 (1978).
29. Candler A.C. *Atomic Spectra and Vector Model* (Cambridge: Cambridge University Press, 1937).
30. Kompaneets A.S. *Kurs teoreticheskoy fiziki* (A Course of Theoretical Physics) (Moscow: Prosveshcheniye, 1972) Vol. 1.
31. Sobel'man I.I. *An Introduction to the Theory of Atomic Spectra* (Oxford: Pergamon Press, 1972).
32. Ilyin A.A., Nagorny I.G., Bukin O.A. *Appl. Phys. Lett*., **96**, 171501 (2010).
33. Ilyin A.A., Bukin O.A., Bulanov A.V. *Tech. Phys*., **53**, 693 (2008) [*Zh. Tekh. Fiz*., **78**, 20 (2008)].
34. Raizer Yu.P. *Lazernaya iskra i rasprostraneniye razryadov* (Laser Spark and Discharge Propagation) (Moscow: Nauka, 1974).
35. Kien F.L., Schneeweiss P., Rauschenbeutel A. *Eur. Phys. J. D*, **67**, 92 (2013).
36. Manakov N.L., Ovsiannikov V.D., Rapoport L.P. *Phys. Rep*., **141**, 320 (1986).
37. Delone N.B., Kraynov V.P. *Phys. Usp*., **42**, 669 (1999) [*Usp. Fiz. Nauk*, **169**, 753 (1999)].
38. Ivković M., Konjević N. *Spectrochim. Acta B*, **131**, 79 (2017).
39. Ilyin A.A., Golik S.S. *Spectrochim. Acta B*, **87**, 192 (2013).